Endocannabinoid Metabolism in the Absence of Fatty Acid Amide Hydrolase (FAAH): Discovery of Phosphorylcholine Derivatives of *N*-Acyl Ethanolamines†

Anke M. Mulder and Benjamin F. Cravatt*

Departments of Cell Biology and Chemistry, The Skaggs Institute for Chemical Biology, The Scripps Research Institute, 10550 North Torrey Pines Road, La Jolla, California 92037

Received June 6, 2006; Revised Manuscript Received July 20, 2006

ABSTRACT: Lipid transmitters are tightly regulated by a balance of biosynthetic and degradative enzymes. Termination of the activity of the *N*-acyl ethanolamine (NAE) class of lipid-signaling molecules, including the endocannabinoid anandamide (AEA), is principally mediated by the integral membrane enzyme fatty acid amide hydrolase (FAAH) *in vivo*. FAAH(−/−) mice are highly sensitized to the pharmacological effects of AEA; however, these animals eventually recover from AEA treatment, implying the existence of alternative routes for NAE metabolism. Here, we have pursued the characterization of these pathways by profiling the metabolome of FAAH(−/−) mice treated with AEA. Multiple AEA-induced metabolites were observed in brains from FAAH(−/−) mice, including a major product with a mass shift of +165 Da (*m/z* 513). The structure of this product was determined to be *O*-phoshorylcholine (PC)−AEA. Analysis of untreated mice identified PC−NAEs as endogenous constituents of the central nervous system (CNS) that were highly elevated in FAAH(−/−) animals. PC−NAEs were very poor substrates for FAAH; however, a vanadate-sensitive enzymatic activity was detected in brain membranes that converted PC−NAEs back to their parent NAEs. The choline-specific phosphodiesterase NPP6 was identified as a candidate enzyme responsible for this activity. These data indicate the presence of a complete metabolic pathway for the production and degradation of PC−NAEs in the CNS that constitutes an alternative route for endocannabinoid metabolism.

Fatty acid amides (FAAs)[1] comprise a large and diverse family of endogenous signaling lipids in mammals. Subclasses of bioactive FAAs include the *N*-acyl ethanolamines (NAEs), such as the endogenous cannabinoid *N*-arachidonoyl ethanolamine (anandamide, AEA) (*1*), the satiating factor *N*-oleoyl ethanolamine (OEA) (*2*), and the anti-inflammatory substance *N*-palmitoyl ethanolamine (PEA) (*3*); the primary FAAs, such as the sleep-inducing lipid oleamide (*4*); and the *N*-acyl amino acids, including *N*-acyl glycines (*5*) and *N*-acyl taurines (NATs) (*6*), which inhibit pain (*5*) and activate TRPV channels (*7*), respectively. The magnitude and duration of FAA signaling is principally regulated *in vivo* by the integral membrane enzyme fatty acid amide hydrolase (FAAH) (*8, 9*). Mice with a targeted disruption of the *FAAH* gene [FAAH(−/−) mice] (*10*) or rodents treated with FAAH inhibitors (*11, 12*) possess highly elevated brain levels of FAAs that correlate with analgesic (*10*−*12*), anxiolytic (*11*), and anti-inflammatory (*12*−*15*) phenotypes. These studies suggest that FAAH may represent an attractive therapeutic target for a range of human disorders (*16*−*18*).

FAAH(−/−) mice are also highly sensitized to the pharmacological effects of AEA, which produces analgesia, hypomotility, catalepsy, and dramatic reductions in body temperature (∼7−8 °C) in these animals (*10*). These effects are blocked by pretreatment with the brain cannabinoid (CB1) receptor antagonist SR141716 (*10*) or transgenic reintroduction of FAAH into the nervous system (*13*), indicating that they are mediated by CB1 receptors expressed in the brain and/or spinal cord. Within about 4 h following treatment with a maximally effective dose of AEA [50 mg/kg, intraperitoneal (i.p.)], FAAH(−/−) mice begin to show signs of recovery and, by 6−8 h, appear relatively normal in terms of cage behavior (*10*). Although this recovery process may be due to the gradual excretion of AEA from the central nervous system (CNS), it could also reflect the existence of additional routes for the metabolism of AEA. To explore this latter possibility, we have conducted a metabolomic analysis of CNS tissues from FAAH(−/−) mice treated with AEA. These studies have led to the discovery of a novel derivative of AEA and other NAEs, the *O*-phosphorylcholine (PC) adducts. PC−NAEs are endogenous constituents of the CNS, highly elevated in FAAH(−/−) mice, and subject to rapid enzymatic catabolism by a vanadate-sensitive phosphodiesterase activity in the brain.

† This work was supported by the National Institutes of Health Grants DA015197 and DA017259 (to B.F.C.), a National Science Foundation Predoctoral Fellowship (to A.M.M.), the Skaggs Institute for Chemical Biology, and the Helen L. Dorris Institute for the Study of Neurological and Psychiatric Disorders of Children and Adolescents.

* To whom correspondence should be addressed. Telephone: (858) 784-8633. Fax: (858) 784-8023. E-mail: cravatt@scripps.edu.

[1] Abbreviations: CB1, brain cannabinoid receptor; CB2, periperhal cannabinoid receptor; DMP, discovery metabolite profiling; FAA, fatty acid amide; FAAH, fatty acid amide hydrolase; IDMS, isotope-dilution mass spectrometry; LC−MS, liquid chromatography−mass spectrometry; NAE, *N*-acyl ethanolamine; PC, phosphorylcholine; SIM, selected ion monitoring.

10.1021/bi061122s CCC: $33.50
Published on Web 09/02/2006

EXPERIMENTAL PROCEDURES

AEA Treatment of FAAH(−/−) Mice, Tissue Isolation, and Sample Preparation. AEA and d_4-ethanolamine−AEA were synthesized from arachidonoyl chloride following previously described procedures (*4*, *8*) and administered (50 mg/kg) in a vehicle of 18:1:1 saline/emulphor/ethanol via i.p. injection to FAAH(−/−) mice (3−6 months of age). Brains, spinal cords, and livers were isolated 2 or 6 h postadministration and stored at −80 °C. Lipids were extracted using a solution of 2:1:1 $CHCl_3$/MeOH/H_2O as described previously (*6*). Concentrated samples were either stored at −80 °C or immediately resuspended in 100 μL of $CHCl_3$ for liquid chromatography−mass spectrometry (LC−MS) analysis.

Discovery Metabolite Profiling (DMP) Analysis of AEA-Treated FAAH(−/−) Mice. LC−MS analysis was performed as described previously (*6*) using an Agilent 1100 LC-MSD SL instrument and a Phenomenex Gemini C18 column (5 μm, 50 × 4.6 mm). Mobile phase A consisted of 95:5 water/methanol, and mobile phase B consisted of 60:35:5 2-propanol/methanol/water; mobile phases contained 0.1% formic acid (positive mode) or ammonium hydroxide (negative mode). Three independent sets of comparisons were performed between AEA-treated and vehicle-treated FAAH(−/−) mice, and the resulting pairs of data sets were analyzed using the XCMS software (http://metlin.scripps.edu) to identify differentially expressed metabolites (*19*). The data sets were further filtered using the following ordered criteria: an average fold change in AEA/vehicle samples of ≥2.5, the presence of the metabolite in all three AEA data sets, and an estimated *p* value from XCMS analysis of <0.15. These criteria reduced the list of mass ions detected by XCMS from ∼1000 to 10−15 candidate differentially expressed metabolites. The extracted ion chromatograms and mass spectra of these 10−15 ions were analyzed manually, and the list was further reduced to three candidate differentially expressed metabolites, *m*/*z* 348 (AEA), 393, and 513, based on the exclusion of ions with manually calculated fold changes less than 2.5 or signals that corresponded to noise peaks. The fold changes and retention times reported for the *m*/*z* 348 (AEA), 393, and 513 ions were calculated manually by normalizing the area of the extracted ion chromatogram (EIC) to the total ion chromatograph (TIC) from 20 to 80 min.

Targeted Analysis of AEA-Treated FAAH(−/−) Mice. Targeted LC−MS analysis was performed for 60 min using the positive-mode mobile phases described above; data was collected in selected ion monitoring (SIM) mode, as described previously (*6*). LC analysis was initiated with an isocratic elution of 100% A at 0.1 mL/min for 5 min, followed by a gradient from 20 to 100% B over 40 min, an isocratic elution of 100% B at 0.5 mL/min for 7 min, and an equilibration in 100% A at 0.5 mL/min for 7 min.

Preparative High-Performance Liquid Chromatography (HPLC) Purification of the m/z 513 Metabolite. Organic extracts of brains and livers from six AEA-treated FAAH(−/−) mice were combined for preparative HPLC purification over a Phenomenex Gemini C18 column (5 μm, 50 × 10 mm) using a Hitachi 7000 series HPLC system as described previously (*6*). Mobile phases A and B were the same as described above and contained 0.1% formic acid solvent modifier. The flow rate was 2.5 mL/min with a 0−100% B gradient over 60 min followed by isocratic elution of 100% B for 20 min. HPLC fractions enriched in the *m*/*z* 513 metabolite were identified by mass analysis, combined, concentrated under a stream of nitrogen, and stored at −80 °C.

Electrospray Ionization−Time of Flight (ESI−TOF) Analysis of the m/z 513 Metabolite. The exact mass of the *m*/*z* 513 metabolite was determined using an Agilent MSD−TOF instrument in dual-spray mode with one of the nebulizers spraying Agilent ESI−TOF tuning mix (part number G1969-8500) and the other spraying eluent from the LC. The tuning mix was used for lock mass calibration and contained fluorocarbons with masses 322.048121, 622.028960, and 922.009798. The capillary voltage was set to 3.5 kV; the fragmentor voltage was set to 120 V; the drying gas temperature was 350 °C; the drying gas flow rate was 5 L/min; and the nebulizer pressure was 6 psi. For LC, a Zorbax SB-C18 column (5 μm, 150 × 0.3 mm) was used with a flow rate of 4 μL/min. Positive-mode (0.1% formic acid) mobile phase A contained 95:5 water/methanol, and mobile phase B contained 60:35:5 isopropanol/methanol/water. The gradient started at 100% A for 5 min and then increased linearly to 100% B over 45 min, followed by an isocratic elution in 100% B for 5 min, and an equilibration in 100% A.

Tandem MS Experiments. MS/MS experiments were performed in the negative-ion mode using a Micromass Q−TOF *Micro* instrument (Manchester, U.K.) equipped with a Z-spray electrospray source and a lockmass sprayer. The source temperature was set to 110 °C with a cone gas flow of 150 L/h, a desolvation gas temperature of 365 °C, and a nebulization gas flow rate of 350 L/h. The capillary voltage was set at 3.2 kV, and the cone voltage was set at 30 V. The collision energy was set at 40−45 V. Samples were directly infused for acquisition times of 2 min at 4 L/min using a Harvard Apparatus syringe pump. MS/MS data were collected in the centroid mode over a scan range of *m*/*z* 75−550.

Synthesis of PC−NAEs. PC−NAEs were synthesized from NAEs following general protocols for the synthesis of ether phospholipids (*20*) as described below for PC−OEA.

OEA Synthesis. A solution of oleic acid (600 mg, 2.1 mmol, 1.0 equiv) in CH_2Cl_2 (10 mL) was treated with oxalyl chloride (1.5 mL, 17 mmol, 8.0 equiv), and stirred under argon for 4 h at room temperature. The reaction mixture was concentrated under a stream of nitrogen followed by evaporation under vacuum for 20−60 min. CH_2Cl_2 (6 mL) and 2 mL of ethanolamine (31 mmol, 15.0 equiv) were added to the concentrated solid, and the reaction mixture was stirred vigorously for 30−60 min. The reaction was quenched with 10% HCl and partitioned between CH_2Cl_2 (100 mL) and 10% HCl (100 mL). The aqueous layer was washed with CH_2Cl_2 (100 mL × 3), the organic layer was dried over anhydrous sodium sulfate and concentrated using a rotary evaporator. The resulting solid was purified over a silica gel column using a 50:50 ethyl acetate/hexanes solvent (3 column volumes) to flush the remaining starting material and 100% ethyl acetate to elute OEA (550 mg, 1.7 mmol, 80%). ^{1}H NMR (600 MHz, MeOD) δ: 0.90 (t, 3H, J = 6.95), 1.33 (m, 20H), 1.61 (m, 2H), 2.04 (m, 4H), 2.19 (t, 2H, J = 7.0 Hz), 3.31 (m, 2H), 3.58 (m, 2H), and 5.34 (m, 2H). For preparation of deuterated compounds, the above synthesis

was done on a smaller scale (100 mg of oleic acid, 0.36 mmol, 1.0 equiv), and deuterated (d_4) ethanolamine was added in the presence of base (Et_3N, 1.8 mmol, 5.0 equiv).

PC−OEA Synthesis. OEA (200 mg, 0.62 mmol, 1.0 equiv) and dry benzene (2 mL) were added to a 15 mL round-bottom flask (flame-dried under argon) fitted with a stir bar. While stirring under argon, Et_3N (260 μL, 1.8 mmol, 3.0 equiv) was added, followed by 2-chloro-1,3,2-dioxaphospholane-2-oxide (400 μL, 4.4 mmol, 7.0 equiv). The reaction was stirred under argon for 24 h, after which it was concentrated using a rotary evaporator, and residual solvent was removed under high vacuum for 4−8 h. The resulting yellow oil was used directly in the next step. The oil was dissolved in dry acetonitrile (2 mL) and added under argon to a flame-dried pressure tube fitted with a stir bar. The reaction mixture was cooled to −78 °C in a dry ice/acetone bath, and cooled Me_3N (570 μL, 4.9 mmol, 8.0 equiv) was added. The pressure tube was sealed, warmed to room temperature, and stirred at 65 °C for 48 h. The reaction mixture was concentrated using a rotary vaporator, and the resulting solid was purified over a silica gel column. The column was flushed with 100 mL of 1:4 MeOH/$CHCl_3$ to remove the remaining starting material, and the product was eluted with 65:25:4 $CHCl_3$/MeOH/H_2O. Product fractions were identified via thin-layer chromatography (TLC) (R_f = 0.24; 65:25:4 $CHCl_3$/MeOH/H_2O, stained with ceric ammonium molybdate), combined, and concentrated using a rotary evaporator. The concentrated material was further purified via preparative HPLC over a Clipeus C18 column using 0.1% formic acid mobile phases as described previously (*6*). The flow rate was 5 mL/min, and LC began with an isocratic elution of 100% A for 5 min, followed by a linear gradient of 40−100% B over 60 min, and an isocratic elution of 100% B for 15 min. The LC fractions containing PC−OEA (retention time, 46−48 min) were identified via MS, combined, and concentrated using a rotary evaporator to yield approximately 5.0 mg of pure product (0.17 mmol, 3%). ^{1}H NMR (600 MHz, $CDCl_3$) δ: 0.88 (t, 3H, J = 6.95), 1.30 (m, 20H), 1.56 (m, 2H), 2.03 (m, 4H), 2.17 (t, 2H, J = 7.0), 3.30 (s, 9H), 3.48 (m, 2H), 3.75 (m, 2H), 3.88 (m, 2H), 4.28 (m, 2H), 5.33 (m, 2H), and 6.86 (d, 1H, J = 6.9). HRMS calculated for $C_{25}H_{52}N_2O_5P^+$ (MH+), 491.3608; found, 491.3605; 0.7 ppm.

For PC−AEA, ^{1}H NMR (500 MHz, MeOD) δ: 0.91 (t, 3H, J = 6.95), 1.29 (m, 6H), 1.68 (m, 2H), 2.10 (m, 4H), 2.22 (m, 2H), 2.82 (m, 6H), 3.22 (s, 9H), 3.40 (m, 2H), 3.63 (m, 2H), 3.91 (m, 2H), 4.26 (m, 2H), and 5.35 (m, 8H). HRMS calculated for $C_{27}H_{50}N_2O_5P^+$ (MH+), 513.3452; found, 513.3448; 0.8 ppm.

Note that the scale of synthesis of d_4-PC−NAE was smaller because of limited quantities of starting material (d_4-ethanolamine), and therefore, these reagents were partially purified in a single step by preparative HPLC prior to use. The purity of d_4-PC−NAE in standard samples was estimated by NMR to be 52% based on a NMR of d_4-PC−OEA, with the majority of contaminating material appearing to correspond to phospho-OEA. The percentage of d_4-PC−OEA was quantified by dividing the areas of diagnostic peaks for PC−OEA versus total OEA products at 3.75 and 5.33 ppm, which corresponded to the CH_2N$(CH_3)_3$ and CH=CH protons, respectively. A correction factor of 0.52 was accordingly used in the calculation of absolute PC−NAE levels as described below.

Measurement of Absolute Levels of PC−AEA in AEA-Treated FAAH(−/−) Mice. Mice were treated with AEA (50 mg/kg, i.p.), and isolated tissues were prepared as described above, except for the inclusion of a d_4-PC−AEA standard (30 pmol) in the extraction solution. Targeted LC−MS analysis was conducted as described above, and the concentration of PC−AEA was estimated with respect to the d_4-PC−AEA standard. AEA levels in these samples were calculated on the basis of a standard curve for NAE ionization generated following the lipid extraction and LC−MS scheme described above.

Measurement of Endogenous Levels of PC−NAEs. Tissues were isolated from naive FAAH(+/+) and FAAH(−/−) mice and prepared as described above, except for the inclusion of d_4-PC−AEA (30 pmol), d_4-PC−OEA (100 pmol), d_4-PC−PEA (100 pmol), d_4-AEA (20 pmol), d_4-OEA (200 pmol), and d_4-PEA (200 pmol) standards in the extraction solution. Targeted LC−MS analysis was conducted as described above, except that the gradient increased linearly from 0 to 35% B for 10 min after the first 5 min, followed by a linear gradient from 35 to 80% B over 45 min. The amount of PC−NAEs and NAEs were calculated with respect to their corresponding deuterated standards. Calibration curves with known quantities of PC−OEA and d_4-OEA added to brain samples provided estimated sensitivity limits of detection of 120 and 1 pmol/g of tissue, respectively (defined as mass ion intensity values that were 2-fold above the lowest detectable signals by LC−MS).

FAAH Assays with PC−OEA. FAAH protein purification and hydrolysis assays were performed as described previously (*6*, *21*). Briefly, recombinant rat FAAH protein (5 and 50 nM for assays with OEA and PC−OEA, respectively) was incubated with the inhibitor URB597 (5 μM) or dimethylsulfoxide (DMSO) for 20 min at room temperature, followed by incubation with PC−OEA or OEA (100 μM) at room temperature in 100 μL of 125 mM Tris-HCl, 1 mM ethylenediaminetetraacetic acid (EDTA), and 0.1% Triton X-100 at pH 9.0. Reactions were performed in triplicate and quenched with 50 μL of 0.5 N HCl and diluted to 300 μL with reaction buffer. LC−MS analysis was performed on 30 μL of this solution in negative mode for the detection of the oleic acid product using selected ion monitoring (SIM). The mobile phases were the same as described above, with 0.1% ammonium hydroxide solvent modifier. The amount of oleic acid produced was calculated on the basis of a standard curve for oleic acid ionization at the end of each run.

Conversion of PC−OEA to OEA by Mouse Brain Preparations. The enzymatic catabolism of PC−OEA to OEA by mouse brain homogenates was measured by LC−MS. Brain extracts were prepared by dounce homogenization of FAAH-(+/+) brains in 50 mM Tris-HCl at pH 8.0, followed by centrifugation at 1300*g* for 3 min. The supernatant was separated into soluble and particulate (membrane) fractions via centrifugation at 100000*g* and 4 °C for 45 min using a benchtop ultracentrifuge. The resulting supernatant constituted the soluble fraction, and the pellet was washed (50 mM Tris-HCl at pH 8.0, 3×) and resuspended in 50 mM Tris-HCl at pH 8.0 to give the membrane fraction. Protein concentrations were determined using a Bradford assay.

Membrane and soluble fractions (3.5 mg of protein/mL) were preincubated with URB597 (5 μM) in 100 μL of 50 mM Tris-HCl at pH 8.0 for 20−30 min to prevent degradation of generated OEA. Membrane fractions from FAAH(−/−) brains were prepared and assayed in a similar manner, except that URB597 was not included in these reactions. A portion of each sample was heat-denatured at 95 °C for 10 min. Assays were also conducted in the presence of sodium orthovanadate (Na_3VO_4, 100 μM). Samples were then incubated with PC−OEA (100 μM) for 30, 60, and 90 min, and the reactions were quenched with 500 μL of $CHCl_3$, followed by the addition of 250 μL of MeOH and 250 μL of 50 mM Tris at pH 8.0 to bring the final volume to 1 mL. LC−MS analysis was conducted on 30 μL of the organic phase in positive mode using SIM to follow the accumulation of OEA (*m/z* 326). Mobile phases were as detailed above with 0.1% formic acid solvent modifier. For LC analysis, the flow rate was 0.75 mL/min and started with a linear gradient from 80 to 100% B over 5 min, followed by an isocratic elution of 100% B for 4 min, 80% B for 3 min, and 20% B for 3 min. The amount of OEA produced was calculated on the basis of a standard curve for OEA ionization. The pH-rate profile studies were conducted using FAAH(−/−) brain membranes in a buffer of 50 mM Bis-Tris propane, 50 mM 3-(cyclohexylamino)-1-propanesulfonic acid (CAPS), 50 mM citrate, 150 mM NaCl, and 0.05% Triton X-100. All reactions were performed in triplicate (except reactions at pH 5.0 and 6.0, which were conducted in duplicate) and averaged to provide the data shown in Figures 5 and 6.

Assessment of Binding of PC−AEA to Cannabinoid Receptors. Cannabinoid receptor binding interactions for PC−AEA were determined using a competitive radioligand binding assay ([^{3}H]CP-55,940) and rat whole brain homogenates and transfected Chinese Hamster Ovary (CHO) cells for the CB1 and peripheral cannabinoid (CB2) receptor, respectively, as described previously (*22*).

Characterization of the PC−OEA Phosphodiesterase Activity of NPP6. A full-length clone encoding the human NPP6 cDNA was ordered from Open Biosystems (clone 5259487) and subcloned into the pcDNA3.1 myc-his vector by the polymerase chain reaction (PCR) using the following primers: forward, 5′-GGAGGTACCATGGCAGTGAAGC-3′; reverse, 5′-CGCTCTAGATGCAAGCAGGAAGAGAAG-3′. The human NPP6 shares 86% sequence identity with mouse NPP6 and was selected for analysis because of commercial availability of the corresponding cDNA and evidence from previous studies that these orthologous enzymes share similar substrate selectivities (*23*). The complete NPP6 cDNA was sequenced to confirm that no errors were introduced by PCR. COS−7 cells were transiently transfected with the NPP6-pcDNA3.1 myc-his construct or empty vector (mock) using a FuGene transfection kit (Roche). Cells were grown at 37 °C for 2 days and then harvested by scraping. Cell pellets were dounce-homogenized and sonicated, and membrane and soluble fractions were separated by centrifugation at 100000*g* for 45 min at 4 °C. The membrane fraction was washed 2× and resuspended in 300 μL of 50 mM Tris-HCl at pH 8.0. Activity assays were performed in triplicate as described above.

RESULTS

Metabolite Profiling of Tissues from AEA-Treated FAAH-(−/−) Mice. Global metabolite profiles of tissues from AEA (50 mg/kg, i.p.) and vehicle-treated FAAH(−/−) mice were compared using an untargeted LC−MS method. This technique, referred to as discovery metabolite profiling (DMP) (*6*), analyzes small molecules across a broad mass range (200−1200 mass units) and uses mass ion intensity measurements to estimate their relative levels. DMP analysis was conducted at 2 and 6 h following treatment with AEA to allow sufficient time for the accumulation of metabolic products of this endocannabinoid. These time points also corresponded to periods where the pharmacological effects of AEA in FAAH(−/−) mice were maximal and mostly dissipated, respectively (*10*).

Multiple metabolites were elevated in brains from AEA-treated FAAH(−/−) mice compared to vehicle controls, including AEA itself (*m/z* 348) and compounds with *m/z* values of 393 and 513 (Figure 1A and Table 1). Treatment of FAAH(+/+) mice did not lead to significant accumulation of these metabolites (data not shown), presumably because of rapid hydrolysis of AEA by FAAH. The AEA-induced metabolites did not appear to belong to a standard class of lipids, such as free fatty acids, phospholipids, or monoacylglycerols, because these species were unaltered in AEA-treated FAAH(−/−) mice (Table 1). To discern which of the induced metabolites were direct products of AEA, we administered a deuterated (d_4) version of this NAE to FAAH-(−/−) mice, which led to the accumulation of the corresponding +4 ion for the *m/z* 513 metabolite (Figure 1B). The +4 version of the *m/z* 393 metabolite was not observed in these studies (data not shown), which might suggest that this compound is not a direct product of AEA. However, the signal intensity of the *m/z* 393 ion was quite low, and it is possible that the deuterated version of this metabolite fell below the sensitivity limit of our DMP experiments. Comparative analysis of data sets derived from 2 and 6 h treatments with AEA revealed that the *m/z* 513 ion continued to accumulate over this time course, while AEA conversely declined in abundance (Figure 2A). We therefore pursued the isolation and structural characterization of the *m/z* 513 ion from FAAH(−/−) mice treated with AEA for 6 h.

Isolation and Structural Characterization of the AEA-Derived m/z 513 Product as O-PC−AEA. Targeted LC−MS analysis detected the *m/z* 513 metabolite in both CNS and peripheral (e.g., liver) tissues of AEA-treated FAAH-(−/−) mice (Figure 2B). We therefore purified this compound from the combined organic extracts of brain and liver tissues of AEA-treated FAAH(−/−) mice using preparative HPLC. The exact mass of the metabolite was determined by ESI−TOF LC−MS to be 513.3445, affording a predicted molecular formula of either $C_{27}H_{50}N_2O_5P$ or $C_{31}H_{47}NO_5$ (each within 2.5 ppm of the measured exact mass). Tandem MS generated a fragmentation pattern for the metabolite that included a major ion of *m/z* 184 and minor ions of *m/z* 86, 104, 125, 147, and 168 (Figure 3A). The *m/z* 184 fragment was indicative of the presence of a PC group (*24*), suggesting that the metabolite could represent the *O*-PC derivative of AEA (molecular formula of $C_{27}H_{50}N_2O_5P$; Figure 3B). This structural prediction was confirmed by a comparison of the properties of the natural metabolite and synthetic PC−AEA,

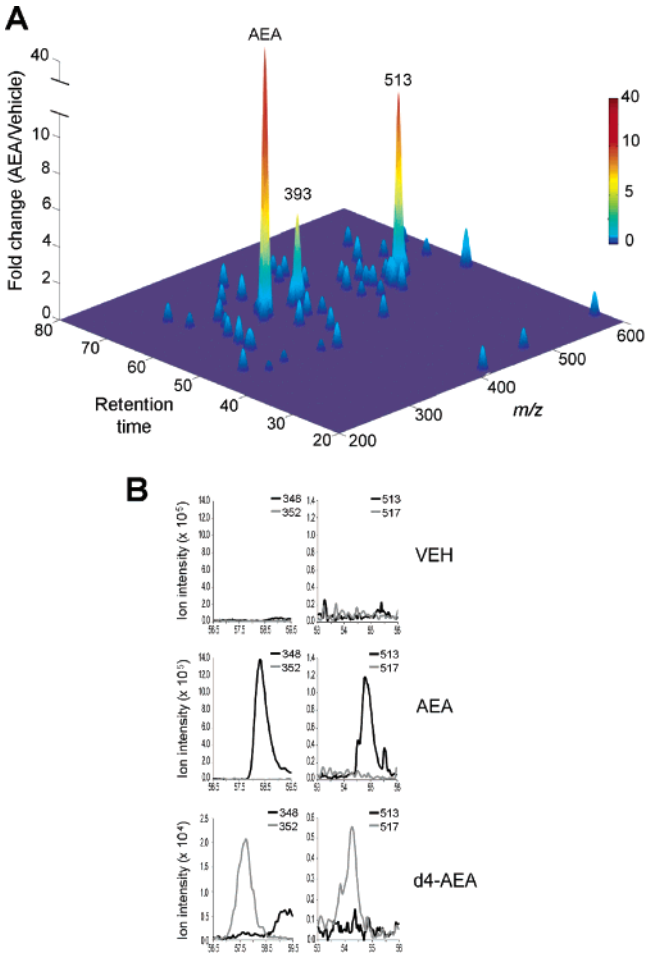

FIGURE 1: AEA metabolism in brains from FAAH(−/−) mice. (A) DMP analysis of brain metabolomes from AEA-treated (50 mg/kg, i.p.) and vehicle-treated FAAH(−/−) mice. Animals were treated with AEA for 6 h prior to analysis. Metabolites are plotted over a mass range of 200−600 Da and LC retention times of 20−80 min (plot shown for positive ionization mode). Multiple metabolites were elevated in FAAH(−/−) brains, including AEA and compounds of masses *m*/*z* 393 and 513. See Table 1 for more details on the relative levels of metabolites in AEA-treated and vehicle-treated FAAH(−/−) mice. (B) Treatment of FAAH(−/−) mice with d_4-AEA (50 mg/kg, i.p.; 6 h) led to the accumulation of a compound with *m*/*z* 517, thus confirming that the *m*/*z* 513 compound is a direct metabolite of AEA.

Table 1: Relative Levels of Representative Brain Metabolites Measured by DMP in AEA-Treated versus Vehicle-Treated FAAH(−/−) Mice[a]

metabolites	acyl chain(s)	*m*/*z*	retention time	AEA/vehicle
AEA derivative		513	55.0	10.3[b]
AEA derivative		393	58.4	5.1[b]
NAEs				
	C20:4 (AEA)	348	58.5	44[b]
	C15:0	286	57.9	0.71
	C16:0	300	59.7	1.0
	C18:1	326	60.7	0.97
	C18:0	328	63.2	0.72
MAGs				
	C16:0	331	60.7	0.73
	C18:1	357	61.7	0.54
	C18:0	359	64.6	0.76
	C20:4	381	58.0	0.67
FFAs				
	C16:0	255	43.5	0.68
	C18:1	281	44.2	0.80
	C18:0	283	46.3	0.80
	C20:4	303	42.8	0.91
	C22:6	327	43.3	0.83
phospholipids				
PA	C34:1	699	51.6	0.74
	C36:2	701	53.8	0.80
PE	C34:1	716	67.0	0.68
	C36:3	742	68.4	0.71
	C36:2	744	71.2	0.47
PC	C36:2	786	56.3	0.73
PS	C36:2	788	60.0	0.68

[a] MAGs, monoacyl glycerols; FAAs, free fatty acids; PA, phosphatidic acid; PE, phosphatidylethanolamine; PC, phosphatidylcholine; PS, phosphatidylserine. Data represent the mass ion intensity ratios of the averages of three independent experiments per group. [b] $p < 0.05$ for AEA-treated versus vehicle-treated samples.

which exhibited identical retention times by LC (Figure 3C) and equivalent fragmentation patterns by MS/MS analysis (Figure 3A).

The absolute levels of PC−AEA generated in AEA-treated FAAH(−/−) mice were measured by isotope-dilution MS (IDMS) using a synthetic d_4 standard. PC−AEA levels in the brains and spinal cords of FAAH(−/−) mice were 102 and 292 pmol/g of tissue, respectively, at 6 h post-treatment with AEA (Figure 4). Interestingly, these values were 15−25% of the levels of AEA observed at this time point (Figure 4), indicating that, in the absence of FAAH, a substantial fraction of AEA is derivatized with PC. Consistent with this route serving as an alternative means to inactivate the signaling function of NAEs, we found that PC−AEA does not act as an agonist for cannabinoid receptors (data not shown).

PC−NAEs Are Endogenous Constituents of the CNS That Are Highly Elevated in FAAH(−/−) Mice. We next investigated whether PC−NAEs might be endogenous metabolites of the CNS. For these studies, we assayed for the presence of not only PC−AEA but also the PC adducts of OEA and PEA, which represent two of the most abundant NAEs in brain tissue (*6*). IDMS analysis identified PC−OEA and PC−PEA in the spinal cords of FAAH(−/−) mice but not FAAH(+/+) mice (Table 2). PC−OEA was also identified in the brains of FAAH(−/−) mice, while PC−PEA could not be detected in this CNS region because of a comigrating contaminating mass. PC−AEA could not be detected in either set of samples, which may reflect the markedly lower endogenous concentrations of its parent NAE (Table 2). The absolute levels of PC−OEA and PC−PEA in spinal cords of FAAH(−/−) mice were 2.2 and 1.6 nmol/g, respectively. On the basis of the sensitivity limit for the detection of PC−OEA by LC−MS (~120 pmol/g of tissue), we estimate that PC−OEA and PC−PEA are at least 20-fold elevated in the CNS of FAAH(−/−) mice compared to FAAH(+/+) mice. The levels of PC−OEA and PC−PEA in the spinal cord of FAAH(−/−) mice were within 20−50% of those observed for the corresponding NAEs (Table 2), indicating that the PC−NAE pathway represents a major route for endogenous NAE metabolism in the absence of FAAH.

We also tested whether PC−NAEs accumulated in the CNS of FAAH(+/+) mice following acute inactivation with the FAAH inhibitor URB597 (*11*). Treatment of FAAH(+/+) mice with URB597 under conditions that cause a significant rise in NAE levels in the CNS (10 mg of URB597/kg, i.p., 2 h) did not lead to detectable levels of PC−NAEs (data not shown). These results suggest that PC−

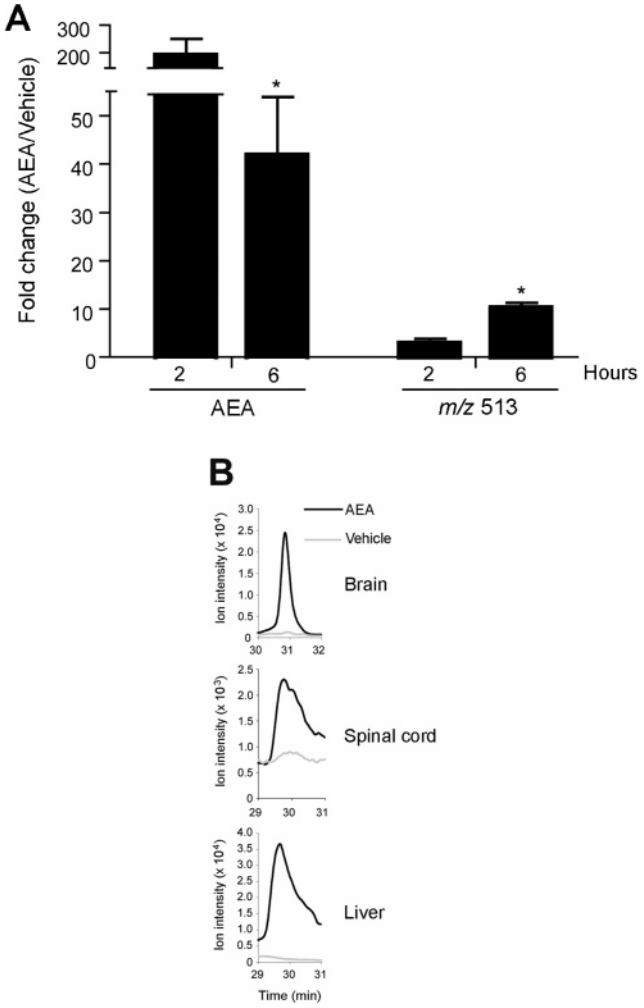

FIGURE 2: Characterization of the distribution of the *m*/*z* 513 metabolite of AEA. (A) *m*/*z* 513 metabolite is present at higher levels in brains of FAAH(−/−) mice treated with AEA for 6 h compared to 2 h. Conversely, AEA levels are significantly reduced at 6 h compared to 2 h (*, $p < 0.05$, planned comparison). $n = 3$ sample/group. (B) *m*/*z* 513 metabolite is detected in multiple tissues from AEA-treated FAAH(−/−) mice, including the brain, spinal cord, and liver.

NAEs, like certain other FAAH-regulated metabolites [e.g., NATs (*7*)], may accumulate slowly in the CNS of inhibitor-treated mice such that the steady-state increases observed in FAAH(−/−) mice are only achieved following prolonged time periods of enzyme inactivation.

An Enzymatic Pathway for PC−NAE Catabolism in Mouse Brain. The identification of PC−NAEs as natural products of the CNS suggested that an enzymatic pathway might exist to catabolize these compounds. One possibility is that FAAH would accept PC−NAEs as direct substrates, hydrolyzing these lipids to their corresponding fatty acids and PC−ethanolamine. To test this premise, purified recombinant FAAH was incubated with PC−OEA and oleic acid formation was measured using an LC−MS assay. FAAH showed only a trace ability to hydrolyze PC−OEA with an initial rate of 7 nmol min^{-1} (mg of FAAH protein)$^{-1}$, which was nearly 100-fold slower than the rate of hydrolysis of a preferred substrate OEA [620 nmol min^{-1} (mg of FAAH protein)$^{-1}$] (Figure 5). We next screened for the existence of additional enzymatic routes for PC−NAE catabolism by incubating PC−OEA with wild-type brain extracts. These assays were run in the presence of the FAAH inhibitor URB597 (*11*) to prevent the degradation of OEA that might be generated as a product of PC−OEA catabolism. PC−OEA was rapidly converted to OEA and PC by brain extracts in a reaction that was heat-sensitive, predominantly associated with membranes, and inhibited by vanadate (parts A and B of Figure 6). Similar results were obtained using brain tissue from FAAH(−/−) mice (data not shown). These results indicate that brain tissue possesses a membrane-associated phosphodiesterase enzyme capable of catabolizing PC−OEA. This PC−OEA phosphodiesterase activity showed a pH optimum of 8.0−9.0 (Figure 6C). Notably, the PC−OEA phosphodiesterase activity [27 pmol min^{-1} (mg of protein)$^{-1}$] was much greater than the predicted rate of FAAH-catalyzed hydrolysis of PC−OEA in brain membranes [1.0 pmol min^{-1} (mg of protein)$^{-1}$] based on estimates of the amount of FAAH in this fraction (∼2 pmol of FAAH/mg of protein) measured by active-site titration with a fluorescent fluorophosphonate probe (*25*, *26*).

In considering candidate enzymes that might convert PC−OEA to OEA, a search of the literature identified nucleotide pyrophosphatase/phosphodiesterase family member 6 (NPP6) as a choline-specific phosphodiesterase (*23*). COS-7 cells transiently transfected with the human NPP6 cDNA displayed robust PC−OEA phosphodiesterase activity compared to mock-transfected cells (Figure 7). The biochemical properties of recombinant NPP6 mirrored closely those displayed by the brain PC−OEA phosphodiesterase activity, including association with membranes (Figure 6A and ref *23*), vanadate sensitivity (Figure 6B and ref *23*), and optimal activity at basic pH (Figure 6C and ref *23*). These results indicate that NPP6 may contribute to PC−NAE catabolism in the brain.

DISCUSSION

The primary role that FAAH plays in regulating NAE levels *in vivo* is supported by a large body of genetic and pharmacological evidence. For example, mice with a disrupted *FAAH* gene (*10*) or treated with FAAH inhibitors (*11*, *12*) possess highly elevated brain levels of NAEs and exhibit analgesic, anxiolytic, and anti-inflammatory phenotypes (*10*−*15*). These studies have engendered the concept of an endogenous NAE tone, where the steady-state level of these lipid-signaling molecules is set by a balance in the activities of biosynthetic and degradative enzymes. A shift in this tone by, for example, inhibition of FAAH then leads to specific NAE-mediated behavioral effects. Despite these advances in our understanding of NAE degradation, we still know very little about the metabolism of these lipids in the absence of FAAH. The presence of alternative routes for NAE metabolism is circumstantially supported by pharmacological studies in FAAH(−/−) mice, whose highly exaggerated behavioral responses to AEA are rectified within 4−6 h postadministration (*10*). Several other enzyme activities have been suggested to participate in AEA degradation, including additional hydrolases (*27*), lipoxygenases (*28*), and cyclooxygenases (*29*). Nonetheless, the contribution made by these enzymes, as well as potentially uncharacterized pathways, to AEA/NAE metabolism *in vivo* remains unknown.

Here, we have pursued the characterization of FAAH-independent routes for AEA metabolism by profiling the

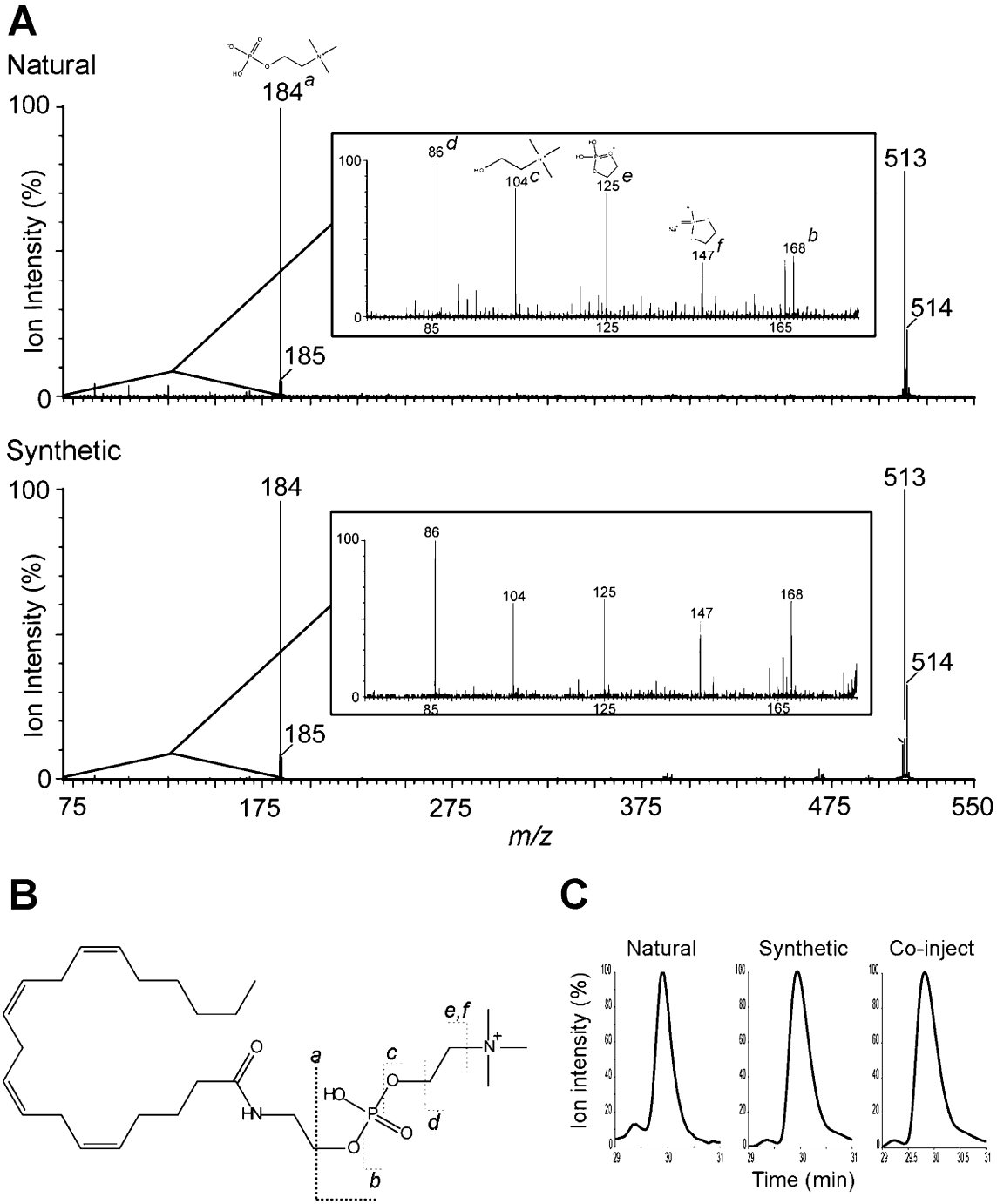

FIGURE 3: Structural characterization of the *m*/*z* 513 metabolite as the *O*-PC derivative of AEA. (A) MS/MS analysis of the natural *m*/*z* 513 metabolite [purified from tissues of AEA-treated FAAH(−/−) mice] and synthetic PC−AEA. Highlighted are a prominent fragment corresponding to PC (*m*/*z* 184) and ions characteristic of PC fragmentation (a−e) (*24*, *35*, *36*). (B) Structure of PC−AEA, with sites of MS fragmentation highlighted (a−e). (C) Comigration by LC−MS of the natural and synthetic samples of PC−AEA.

products of this NAE in brains from FAAH(−/−) mice. These studies employed an untargeted LC−MS analysis platform [DMP (*6*)] to broadly survey the metabolites derived from AEA *in vivo*. A primary metabolic product of AEA was detected in CNS tissue of FAAH(−/−) mice and structurally characterized as the *O*-PC adduct of this NAE. PC−NAEs were further identified as endogenous constituents of the mammalian CNS that are highly elevated in FAAH-(−/−) mice. To our knowledge, these findings provide the first evidence that *O*-PC adducts of NAEs are natural products. When coupled with the recent discovery of several other classes of *N*-fatty acyl derivatives, including *N*-acyl amino acids (*5*) and taurines (*6*), these findings underscore the rich structural diversity of amidated lipids present in mammalian tissues. Interestingly, amidated lipids appear to segregate into at least two groups based on their rates of accumulation in FAAH-inactivated animals. One class, including the NAEs and polyunsaturated NATs, rapidly increase [in the CNS and peripheral tissues, respectively (*7*)] within 1−2 h following FAAH inhibition. The second set of amidated lipids, including saturated NATs and PC−NAEs, appear to require the constitutive inactivation of FAAH to accumulate to significant levels *in vivo*. Such findings emphasize our growing appreciation of the different meta-

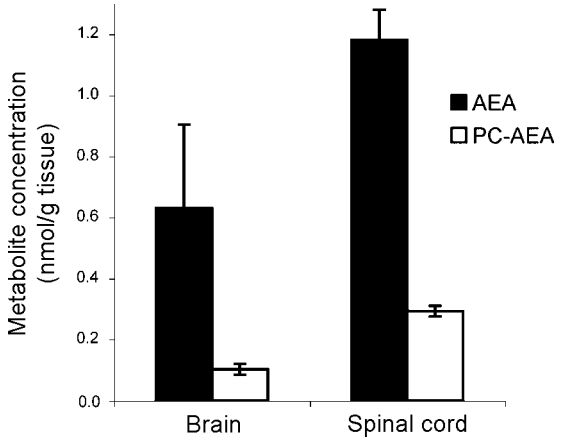

FIGURE 4: Absolute levels of PC−AEA and AEA in CNS tissues from FAAH(−/−) mice treated with AEA (50 mg/kg, i.p.). Levels were determined 6 h after administration of AEA. $n = 3$ sample/group.

Table 2: Levels of PC−NAEs in the CNS of FAAH(+/+) and FAAH(−/−) Mice

tissue	PC−NAE	FAAH(−/−) (pmol/g of tissue)	FAAH(+/+) (pmol/g of tissue)
spinal cord			
	PC−OEA	2200 ± 410[a]	ND[b]
	PC−PEA	1630 ± 340[a]	ND
	PC−AEA	ND	ND
	OEA	4330 ± 100[a]	240 ± 22
	PEA	7550 ± 1660[a]	980 ± 140
	AEA	110 ± 9[a]	3.6 ± 0.5
brain			
	PC−OEA	150 ± 9	ND
	PC−PEA	ND	ND
	PC−AEA	ND	ND
	OEA	920 ± 35[a]	88 ± 15
	PEA	3160 ± 42[a]	326 ± 36
	AEA	35 ± 1[a]	5 ± 1

[a] $p < 0.01$ [planned comparison, where (+/+) values for PC−NAEs were set to the limit of detection for PC−OAE (120 pmol/g of tissue)]; $n = 3$ samples/group. [b] ND = not detected.

bolic phenotypes that emerge following acute versus chronic inactivation of FAAH and may be relevant when interpreting behavioral phenotypes (as well as potential toxicities) that are observed following short-term versus long-term inhibition of this enzyme.

The absolute levels of PC−NAEs were within 20−30% of the levels of NAEs in the CNS of FAAH(−/−) mice, indicating that a substantial fraction of the endogenous NAE pool is converted to PC derivatives in these tissues. How might this chemical transformation occur? PC−NAE biosynthesis could be accomplished by the enzymatic coupling of cytidine 5′-diphosphate (CDP)−choline to NAEs in a reaction analogous to the formation of PC from CDP−choline and diacylglycerol. There are at least two enzymes in mammals that catalyze this reaction termed cholinephosphotransferase 1 (*30*) and choline/ethanolaminephosphotransferase 1 (*31*), and it will be interesting to determine if either of these proteins can form PC−NAEs.

Although the precise biosynthetic pathway for PC−NAEs remains unclear, a potential enzymatic route for their degradation was detected. This vanadate-sensitive phosphodiesterase activity was found predominantly on membranes and catalyzed the conversion of PC−NAEs back to

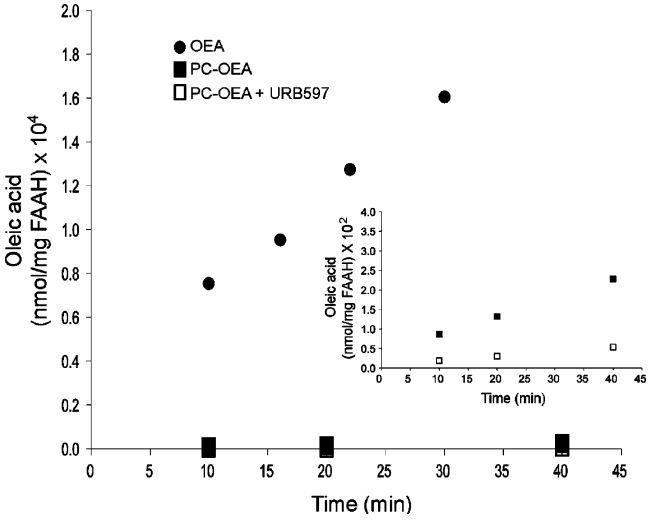

FIGURE 5: PC−NAEs are poor substrates for FAAH. A comparison of the hydrolysis of PC−OEA and OEA by purified, recombinant FAAH. From these data, initial rates were calculated for FAAH-catalyzed hydrolysis of PC−OEA and OEA of 7 and 620 nmol min^{-1} (mg of FAAH)$^{-1}$, respectively. All data represent the average of three independent experiments, for which standard errors were less than 15%.

their parent NAEs. The PC−NAE phosphodiesterase activity greatly exceeded the predicted level of FAAH-catalyzed hydrolysis of PC−NAEs in brain, designating the former pathway as a stronger candidate for controlling the catabolism of these lipids *in vivo*. As a corollary, we interpret the elevated levels of PC−NAEs observed in the CNS of FAAH(−/−) mice to derive from secondary metabolism of heightened concentrations of NAEs rather than protection from FAAH-catalyzed hydrolysis. These findings thus provide the first evidence that disruption of FAAH activity *in vivo* leads to alterations in not only the direct substrates of this enzyme (NAEs), but also their secondary metabolites (PC−NAEs). Finally, the choline-specific phosphodiesterase NPP6 (*23*) was found to convert PC−OEA to OEA in a vanadate-sensitive manner, indicating that this enzyme may play a role in PC−OEA catabolism in the CNS. A summary comparing the pathways for NAE metabolism in FAAH(+/+) and FAAH(−/−) mice is provided in Figure 8. Enzymes that display biochemical activities consistent with participation in this network are highlighted.

We should emphasize that our results do not rule out the contribution of additional enzymes, such as lipoxygenases (*28*) and cyclooxygenases (*29*), to the metabolism of AEA *in vivo*. The products of these enzymes may have been too low in abundance for detection using DMP methods. These oxygenases may also play a larger role in AEA metabolism in peripheral tissues, which were not examined in this study. Another important question is whether the formation of PC−NAEs is relevant to brain metabolism and physiology in wild-type animals or, alternatively, only in the absence of FAAH. Our inability to detect PC−NAEs in whole brain or spinal cord tissues from FAAH(+/+) mice (even after the acute inhibition of FAAH for 2 h) might argue against a role for these lipids in normal CNS function. However, the sensitivity limit for the detection of PC−NAEs by LC−MS was much poorer than for NAEs [∼60−120 versus 1 pmol/g of tissue (*6*), respectively], suggesting that the former class of lipids may have eluded detection in FAAH(+/+) samples.

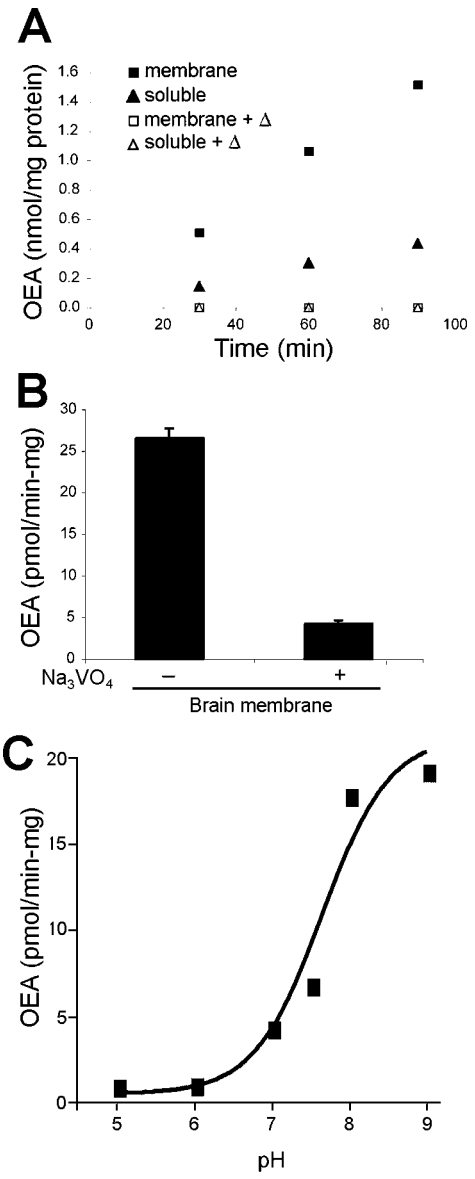

FIGURE 6: Characterization of a phosphodiesterase activity in brain tissue that converts PC−OEA to OEA. (A and B) PC−OEA phosphodiesterase activity was predominantly found in the membrane fraction (A) and was blocked by preheating (Δ) (A) or the phosphodiesterase inhibitor sodium vanadate (Na_3VO_4) (B). (C) pH-rate profile for brain PC−OEA phosphodiesterase activity. All data represent the average of three independent experiments (except for assays conducted at pH 5 and 6, which were performed in duplicate), for which standard errors were less than 15%.

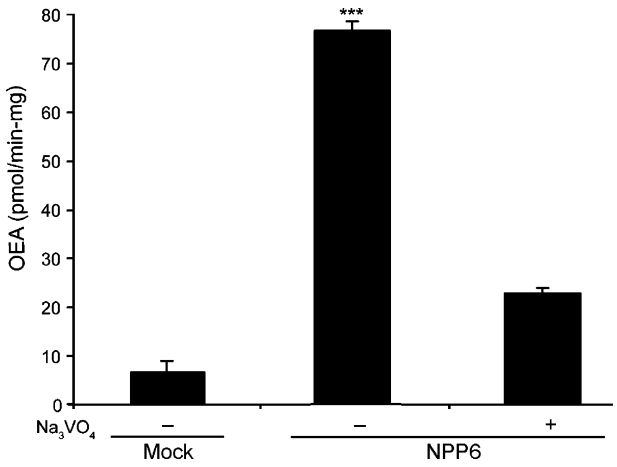

FIGURE 7: Identification of NPP6 as an enzyme with PC−OEA phosphodiesterase activity. COS-7 cells transfected with the NPP6 cDNA exhibited significantly greater PC−OEA phosphodiesterase activity compared to mock-transfected cells. The NPP6-catalyzed conversion of PC−OEA to OEA was blocked by vanadate (Na_3VO_4). ***, $p < 0.001$ for NPP6-tranfected versus mock-transfected or vanadate-treated NPP6-transfected cells. All data represent the average of three independent experiments.

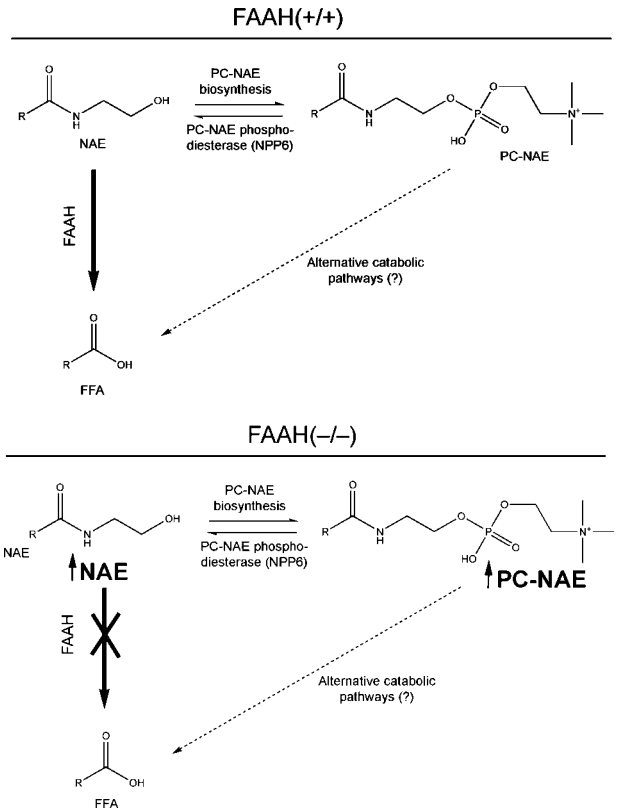

FIGURE 8: Schematic model comparing the catabolic pathways for NAEs in the CNS of FAAH(+/+) and FAAH(−/−) mice. In FAAH(+/+) mice, NAEs (and indirectly PC−NAEs) are tightly controlled by FAAH. In FAAH(−/−) mice, NAEs are highly elevated in the CNS, leading to the accumulation of PC−NAEs through an as of yet undefined biosynthetic pathway. PC−NAEs can in turn be catabolized by a phosphodiesterase activity that may correspond to the choline-specific enzyme NPP6. Other potential metabolic pathways for PC−NAEs may exist, including amide hydrolysis, although these lipids were found to be very poor substrates for FAAH *in vitro* (see Figure 5).

It is also possible that PC−NAEs are only produced in specific neuronal circuits or brain regions, in which case their detection may have been obscured in analyses of whole tissues. If these locations happened to correlate with regions where FAAH activity is low or absent (*32*), then the PC−NAE pathway could constitute an important route for the termination of endocannabinoid signals. Finally, PC−NAEs may remain low under healthy, nonstimulated conditions but accumulate in situations of pathophysiology, as has been observed for NAEs (*33*).

In summary, we have presented data to support the existence of a novel class of amidated lipids in the mammalian CNS, the PC−NAEs, that constitutes a major route for endocannabinoid metabolism in FAAH-inactivated animals. Whether PC−NAEs are inert metabolites of NAEs or function as signaling molecules themselves merits future investigation. A more thorough understanding of the enzymes involved in PC−NAE metabolism and the development of

strategies for their selective inactivation should assist in addressing this question. In the event that PC−NAEs exhibit biological activity, the results of this study may prove instructive for researchers interested in understanding the long-term physiological consequences of FAAH inactivation. Indeed, FAAH(−/−) mice display some behavioral effects that are not rectified by cannabinoid receptor antagonists (*13*, *34*), and it is worth considering whether these phenotypes may be due to alterations in metabolic pathways downstream of the primary substrates of the enzyme.

ACKNOWLEDGMENT

We thank A. Saghatelian for synthetic assistance, Sunia Trauger (HRMS) and Elizabeth J. Want (MS/MS) for assistance in the structural characterization of PC−AEA, A. Lichtman for assistance in determining the cannabinoid receptor activity of PC−AEA, and the Cravatt lab for helpful discussions and critical reading of the manuscript.

REFERENCES

1. Devane, W. A., Hanus, L., Breuer, A., Pertwee, R. G., Stevenson, L. A., Griffin, G., Gibson, D., Mandelbaum, A., Etinger, A., and Mechoulam, R. (1992) Isolation and structure of a brain constituent that binds to the cannabinoid receptor, *Science 258*, 1946−1949.
2. Rodriguez de Fonseca, F., Navarro, M., Gomez, R., Escuredo, L., Nava, F., Fu, J., Murillo-Rodriguez, E., Giuffrida, A., LoVerme, J., Gaetani, S., Kathuria, S., Gall, C., and Piomelli, D. (2001) An anorexic lipid mediator regulated by feeding, *Nature. 414*, 209−212.
3. Lambert, D. M., Vandevoorde, S., Jonsson, K. O., and Fowler, C. J. (2002) The palmitoylethanolamide family: a new class of anti-inflammatory agents? *Curr. Med. Chem. 9*, 663−674.
4. Cravatt, B. F., Prospero-Garcia, O., Siuzdak, G., Gilula, N. B., Henriksen, S. J., Boger, D. L., and Lerner, R. A. (1995) Chemical characterization of a family of brain lipids that induce sleep, *Science 268*, 1506−1509.
5. Huang, S. M., Bisogno, T., Petros, T. J., Chang, S. Y., Zavitsanos, P. A., Zipkin, R. E., Sivakumar, R., Coop, A., Maeda, D. Y., De Petrocellis, L., Burstein, S., Di Marzo, V., and Walker, J. M. (2001) Identification of a new class of molecules, the arachidonyl amino acids, and characterization of one member that inhibits pain, *J. Biol. Chem. 276*, 42639−42644.
6. Saghatelian, A., Trauger, S. A., Want, E. J., Hawkins, E. G., Siuzdak, G., and Cravatt, B. F. (2004) Assignment of endogenous substrates to enzymes by global metabolite profiling, *Biochemistry 43*, 14332−14339.
7. Saghatelian, A., McKinney, M. K., Bandell, M., Smith, C. A., Patapoutian, A., and Cravatt, B. F. (2006) FAAH regulated fatty *N*-acyl taurines (NATs) activate TRPV4 ion channel, *Biochemistry 45*, 9007−9015.
8. Cravatt, B. F., Giang, D. K., Mayfield, S. P., Boger, D. L., Lerner, R. A., and Gilula, N. B. (1996) Molecular characterization of an enzyme that degrades neuromodulatory fatty-acid amides, *Nature 384*, 83−87.
9. McKinney, M. K., and Cravatt, B. F. (2005) Structure and function of fatty acid amide hydrolase, *Annu. Rev. Biochem. 74*, 411−432.
10. Cravatt, B. F., Demarest, K., Patricelli, M. P., Bracey, M. H., Giang, D. K., Martin, B. R., and Lichtman, A. H. (2001) Supersensitivity to anandamide and enhanced endogenous cannabinoid signaling in mice lacking fatty acid amide hydrolase, *Proc. Natl. Acad. Sci. U.S.A. 98*, 9371−9376.
11. Kathuria, S., Gaetani, S., Fegley, D., Valino, F., Duranti, A., Tontini, A., Mor, M., Tarzia, G., La Rana, G., Calignano, A., Giustino, A., Tattoli, M., Palmery, M., Cuomo, V., and Piomelli, D. (2003) Modulation of anxiety through blockade of anandamide hydrolysis, *Nat. Med. 9*, 76−81.
12. Lichtman, A. H., Leung, D., Shelton, C., Saghatelian, A., Hardouin, C., Boger, D., and Cravatt, B. F. (2004) Reversible inhibitors of fatty acid amide hydrolase that promote analgesia: Evidence for an unprecedented combination of potency and selectivity, *J. Pharmacol. Exp. Ther. 311*, 441−448.
13. Cravatt, B. F., Saghatelian, A., Hawkins, E. G., Clement, A. B., Bracey, M. H., and Lichtman, A. H. (2004) Functional disassociation of the central and peripheral fatty acid amide signaling systems, *Proc. Natl. Acad. Sci. U.S.A. 101*, 10821−10826.
14. Massa, F., Marsicano, G., Hermann, H., Cannich, A., Monory, K., Cravatt, B. F., Ferri, G.-L., Sibaev, A., Storr, M., and Lutz, B. (2004) The endogenous cannabinoid system protects against colonic inflammation, *J. Clin. Invest. 113*, 1202−1209.
15. Holt, S., Comelli, F., Costa, B., and Fowler, C. J. (2005) Inhibitors of fatty acid amide hydrolase reduce carrageenan-induced hind paw inflammation in pentobarbital-treated mice: Comparison with indomethacin and possible involvement of cannabinoid receptors, *Br. J. Pharmacol. 146*, 467−476.
16. Cravatt, B. F., and Lichtman, A. H. (2003) Fatty acid amide hydrolase: An emerging therapeutic target in the endocannabinoid system, *Curr. Opin. Chem. Biol. 7*, 469−475.
17. Gaetani, S., Cuomo, V., and Piomelli, D. (2004) Anandamide hydrolysis: A new target for anti-anxiety drugs? *Trends Mol. Med. 9*, 474−478.
18. Bari, M., Battista, N., Fezza, F., Gasperi, V., and Maccarrone, M. (2006) New insights into endocannabinoid degradation and its therapeutic potential, *Mini-Rev. Med. Chem. 6*, 257−268.
19. Smith, C. A., Want, E. J., O'Maille, G., Abagyan, R., and Siuzdak, G. (2006) XCMS: Processing mass spectrometry data for metabolite profiling using nonlinear peak alignment, matching, and identification, *Anal. Chem. 78*, 779−787.
20. Kazi, A. B., Shidmand, S., and Hajdu, J. (1999) Stereospecific synthesis of functionalized ether phospholipids, *J. Org. Chem. 64*, 9337−9347.
21. Patricelli, M. P., Lashuel, H. A., Giang, D. K., Kelly, J. W., and Cravatt, B. F. (1998) Comparative characterization of a wild type and transmembrane domain-deleted fatty acid amide hydrolase: Identification of the transmembrane domain as a site for oligomerization, *Biochemistry 37*, 15177−15187.
22. Lichtman, A. H., Hawkins, E. G., Griffin, G., and Cravatt, B. F. (2002) Pharmacological activity of fatty acid amides is regulated, but not mediated by fatty acid amide hydrolase *in vivo*, *J. Pharmacol. Exp. Ther. 302*, 73−79.
23. Sakagami, H., Aoki, J., Natori, Y., Nishikawa, K., Kakehi, Y., Natori, Y., and Arai, H. (2005) Biochemical and molecular characterization of a novel choline-specific glycerophosphodiester phosphodiesterase belonging to the nucleotide pyrophosphatase/phosphodiesterase family, *J. Biol. Chem. 280*, 23084−23093.
24. Reis, A., Domingues, P., Ferrer-Correia, A. J., and Domingues, M. R. (2004) Tandem mass spectrometry of intact oxidation products of diacylphosphatidylcholines: Evidence for the occurrence of the oxidation of the phosphocholine head and differentiation of isomers, *J. Mass Spectrom. 39*, 1513−1522.
25. Jessani, N., Liu, Y., Humphrey, M., and Cravatt, B. F. (2002) Enzyme activity profiles of the secreted and membrane proteome that depict cancer cell invasiveness, *Proc. Natl. Acad. Sci. U.S.A. 99*, 10335−10340.
26. Leung, D., Hardouin, C., Boger, D. L., and Cravatt, B. F. (2003) Discovering potent and selective inhibitors of enzymes in complex proteomes, *Nat. Biotechnol. 21*, 687−691.
27. Tsuboi, K., Sun, Y. X., Okamoto, Y., Araki, N., Tonai, T., and Ueda, N. (2005) Molecular characterization of *N*-acylethanolamine-hydrolyzing acid amidase, a novel member of the choloylglycine hydrolase family with structural and functional similarity to acid ceramidase, *J. Biol. Chem. 280*, 11082−11092.
28. Ueda, N., Yamamoto, K., Yamamoto, S., Tokunaga, T., Shirakawa, E., Shinkai, H., Ogawa, M., Sato, T., Kudo, I., Inoue, K., et al. (1995) Lipoxygenase-catalyzed oxygenation of arachidonylethanolamide, a cannabinoid receptor agonist, *Biochim. Biophys. Acta 1254*, 127−134.
29. Kozak, K. R., Crews, B. C., Morrow, J. D., Wang, L. H., Ma, Y. H., Weinander, R., Jakobsson, P. J., and Marnett, L. J. (2002) Metabolism of the endocannabinoids, 2-arachidonylglycerol and anandamide, into prostaglandin, thromboxane, and prostacyclin glycerol esters and ethanolamides, *J. Biol. Chem. 277*, 44877−44885.
30. Henneberry, A. L., Wistow, G., and McMaster, C. R. (2000) Cloning, genomic organization, and characterization of a human cholinephosphotransferase, *J. Biol. Chem. 275*, 29808−29815.

31. Henneberry, A. L., and McMaster, C. R. (1999) Cloning and expression of a human choline/ethanolaminephosphotransferase: Synthesis of phosphatidylcholine and phosphatidylethanolamine, *Biochem. J. 339*, 291−298.
32. Egertova, M., Giang, D. K., Cravatt, B. F., and Elphick, M. R. (1998) A new perspective on cannabinoid signalling: Complimentary localization of fatty acid amide hydrolase and the CB1 receptor in rat brain, *Proc. R. Soc. London, Ser. B 265*, 2081−2085.
33. Hansen, H. S., Lauritzen, L., Moesgaard, B., Strand, A. M., and Hansen, H. H. (1998) Formation of *N*-acyl-phosphatidylethanolamines and *N*-acylethanolamines: Proposed role in neurotoxicity, *Biochem. Pharmacol. 55*, 719−725.
34. Lichtman, A. H., Shelton, C. C., Advani, T., and Cravatt, B. F. (2004) Mice lacking fatty acid amide hydrolase exhibit a cannabinoid receptor-mediated phenotypic hypoalgesia, *Pain 109*, 319−327.
35. McMahon, J. M., Short, R. T., McCandlish, C. A., Brenna, J. T., and Todd, P. J. (1996) Identification and mapping of phosphocholine in animal tissue by static secondary ion mass spectrometry and tandem mass spectrometry, *Rapid Commun. Mass Spectrom. 10*, 335−340.
36. Kerwin, J. L., Tuininga, A. R., and Ericsson, L. H. (1994) Identification of glycerophospholipids and spingomyelin using electrospray mass spectrometry, *J. Lipid Res. 35*, 1102−1114.

BI061122S